Malaysian Journal of Chemistry, 2024, Vol. 26(3), 476-485
(Special Issue: *3rd Virtual International Symposium on Sciences 2023*)

Kinetic, Isotherm, and Thermodynamic Studies of the Removal of Dissolved Chemical Oxygen Demand (dCOD) from Landfill Leachate by Iron Oxide Nanoparticles (IONPs)

Zaidi Ab Ghani[1]*, Mohd Hafiz Yaacob[1], Lee Sin Ang[1], Mohd Suffian Yusoff[2] and Jamil Mohamed Sapari[3]
[1]Faculty of Applied Sciences, Universiti Teknologi MARA Perlis Branch, 02600 Arau Perlis, Malaysia
[2]School of Civil Engineering, Universiti Sains Malaysia Engineering Campus, 14300 Nibong Tebal, Pulau Pinang, Malaysia.
[3]Universiti Teknologi MARA, Negeri Sembilan Branch, Kuala Pilah Campus, 72000 Kuala Pilah, Negeri Sembilan, Malaysia.
*Corresponding author (e-mail: zaidi433@uitm.edu.my)

This study was conducted to investigate the efficiency of the adsorption of iron oxide nanoparticles (IONPs) for the removal of dissolved chemical oxygen demand (dCOD) in landfill leachate. The IONPs were directly prepared via the sodium borohydride (KBH_4) reduction method. Adsorption kinetics, isotherm, and thermodynamic studies are developed to design the model for dCOD removal. Pseudo-first-order (PFO) and pseudo-second-order (PSO) models have been studied to fit the experimental data. The regression results showed that a PSO model represented the adsorption kinetics more accurately. The Weber–Morris intraparticle diffusion model was used to analyse the adsorption kinetics data. The plot of q_t versus $t^{1/2}$ represents multilinearity, which showed that the adsorption processes occurred in more than one step. Adsorption isotherms were analysed using the Langmuir, Freundlich, Temkin, and Dubinin–Radushkevich (D-R), and isotherms model. Equilibrium data were well fitted to the D-R isotherm model. The Langmuir model was used to calculate the maximum monolayer adsorption, which demonstrated a value of 69.44 mg/g. Thermodynamic parameters, such as free energy changes ($\Delta G°$), enthalpy ($\Delta H°$), and entropy ($\Delta S°$), were evaluated between the temperatures of 25°C and 40°C. The $\Delta G°$ was noticed to have progressively decreased from −10.68, −10.87, −11.07, and −11.27 kJ/mol with increasing temperature. The $\Delta H°$ and $\Delta S°$ values were found to be 1.23 kJ/mol and 39.96 J/mol.K, respectively. The results showed that the overall adsorption process was endothermic and spontaneous. This suggested that the IONPs could be a viable adsorbent in managing higher dCOD problems associated with landfill leachate.

Keywords: Adsorption, isotherm; iron oxide nanoparticles; landfill leachate

Received: January 2024; Accepted: February 2024

Landfill leachate is a liquid that becomes polluted by percolating through the waste within the landfill site [1]. The extraction of nutrients and contaminants by liquid medium from the solid waste will result in leachate. The presence and continuous release of high levels of various contaminants have contributed to severe environmental and aquatic life problems. They may harm humans with kidneys, lungs, and skin problems [2]. Thus, it is highly recommended to remove the leachate pollutants before their final discharge into the environment.

Landfill leachate compositions are mainly composed of organic matter, as well as inorganic and xenobiotic organic compounds [1, 3]. There are significant differences in the types of chemicals present, some of which are the higher levels of COD, NH_3-N, colour, and type of heavy metals. These are the main chemicals that pose environmental threats [4]. The biological breakdown of trash in landfills will slow down considerably as it becomes more stable. This is because bio-refractory compounds called recalcitrant organic matter will form [5]. Hence, the leachate generated is more complicated and impossible to treat via biological processes [6, 7]. The presence of recalcitrant organic matter in landfill leachate hinders the effectiveness of biological processes, both aerobic and anaerobic. To meet regulatory standards for landfill leachate discharge into water bodies, physicochemical techniques can be employed as an alternative for pre- or post-treatment of landfill leachate. The chemical oxygen demand (COD) parameter is often used to indicate the refractory portion of organic substances in leachate from landfills.

Today, different techniques have been used to clean up leachate from landfills. These include advanced oxidation processes, such as Fenton [8, 9], ozonation [10, 11], and electrochemical treatment [12, 13]. Chemical precipitation [14], membrane filtration

---

†Paper presented at the 3rd Virtual International Symposium on Sciences (3rd VISoS 2023)

[15], ion exchange [16, 17], and adsorption [3, 6] are some other ways to clean up leachate from landfills. From the aforementioned techniques, adsorption using activated carbon (AC) is also a well-recognised means of leachate treatment. The adsorption process has emerged as an economical, efficient, and environmentally friendly approach for recalcitrant organic matter removal from landfill leachate. Recently, the increased interest in nanotechnology has resulted in the development of many types of metallic and carbon-based nanomaterials for use as nanosorbents (NS). NS are nanoscale particles from organic or inorganic materials that have a high affinity to adsorb substances [18]. Among the available NS, nanosized metal oxides, such as iron oxide, are classified as the most promising ones for the removal of pollutants from aqueous systems. Iron oxide is cheap and readily available, and it also has a higher affinity than any other metal oxides [19].

Recently, there has been much interest in using iron oxide nanoparticles (IONPs) as an adsorbent because they have unique properties, such as their very small size, high surface-area-to-volume ratio, ability to change their shape, great magnetic strength, and biocompatibility. Based on the above scenario, numerous researchers have used iron oxide as an adsorbent to treat heavy metals [20] and organic compounds in wastewater [21]. However, treating wastewater, such as landfill leachate, requires a deeper understanding. Extensive investigations should be done on their possible applications at existing landfill sites. Therefore, the objectives of the present work are to introduce new adsorbent IONPs and to examine their effectiveness in removing dissolved chemical oxygen demand (dCOD) from landfill leachate via batch adsorption experiments. Adsorption isotherm data were fitted into several isotherm models, such as Langmuir, Freundlich, Temkin, and Dubinin-Radushkevich (D-R). Kinetics and thermodynamic studies were also conducted to obtain further information.

EXPERIMENTAL

Chemicals and Materials

All the chemicals used in this study were of analytical reagent grade unless otherwise stated. $Fe(NO_3)_3.9H_2O$ and $NaBH_4$ were purchased from Merck. Landfill leachate samples used in this study were taken from the Matang landfill site (MLS) in Taiping, Perak, Malaysia. The samples were collected from the active detention pond and immediately transported to the laboratory and stored in darkness at 4°C prior to their use for minimising the chemical and biological changes. The leachate samples were centrifuged with a rotating speed of 10,000 r/min for 15 min and filtrated through glass fibre and membrane (0.45 µm) to remove suspended materials that may react with the dissolved substances, as recommended by Jegadeesan, et al. [13]. The organic matter in the filtrate was identified as dCOD. The dCOD was determined by the closed reflux method [22]. The sample was heated with sulfuric acid and a strong oxidising agent, potassium dichromate, for two hours. Oxidisable organic compounds reacted, thus reducing the dichromate ion ($Cr_2O_7^{2-}$) to green chromic ion (Cr^{3+}) and analysed via the Hach spectrophotometer, DR 3900, at 620 nm.

For the preparation of IONPs, 10 g of $Fe(NO_3)_3.9H_2O$ was dissolved in a 500 mL mixture of 30% ethanol and 70% water. Then, 500 mL of 0.5 M $NaBH_4$ was used as a reducing agent and added into the $Fe(NO_3)_3.9H_2O$ solution dropwise while stirring using a magnetic stirrer, as described by Mossa Hosseini, et al. [23]. After the addition of $NaBH_4$, the solution was stirred for another 30 min. The black precipitates were filtered by vacuum filtration through Whatman (No. 1) filter papers and then washed with ethanol and DI water three times. After drying, the sample was heat-treated at 250°C for 4 h to convert iron into iron oxide. The occurrence of synthetic reaction is as follows (Equation 1).

$$4Fe^{3+}_{(aq)} + 3BH_4 + 9H_2O \rightarrow 4Fe^{o}_{(s)\downarrow} + 3H_2BO_3 + 12H^{+}_{(aq)} + 6H_{2(g)\uparrow} \qquad \text{Equation (1)}$$

Adsorbent Characterisation

The surface morphologies of IONPs were examined using Extreme High Resolution Field Emission Scanning Electron Microscope (XHR-FESEM), Model FEI Verios 460L, equipped with Energy-dispersive X-ray spectroscopy (EDS) analysis. Transmission electron microscope (TEM) Philips CM12 with Docu Version 3.2 image analysis were used to further examine the IONPs samples. The surface area of AC produced was characterised by nitrogen gas (N_2) adsorption at −196°C using ASAP 2010, Micromeritics. Transform Infrared (FTIR) spectroscopy with potassium bromide (KBr) pellet technique was applied for the functional group identification. The IR spectra were recorded on Frontier from Perkin Elmer in the range 4000–400 cm^{-1} at resolution 2 cm^{-1}.

Adsorption Study

The batch adsorption studies were carried out by adding 100 mL of MLS leachate with a fixed initial concentration of dCOD (360 mg/L), pH of 8.5 (no adjustments were made in the pH) to different adsorbent dosage (0.5 to 1.75 g). The samples were shaken in a shaker and kept in isothermal at room temperature (25°C ± 2°C) with the shaking speed at 125 rpm within 24 h to reach the equilibrium condition. Then, the samples were taken out and filtered using a0.45-µm nylon membrane before analysis to minimise the interference of the adsorbent. Next, the samples were taken from the filtered solution for dCOD uptake analysis at different parameters. The adsorption capacity of dCOD in the aqueous solution was calculated by using Equation (2) as follows:

$$q_e = \left[(C_o - C_e)V\right] / W \qquad \text{Equation (2)}$$

where, C_e (mg/L) and C_0 (mg/L) represent the equilibrium and initial concentration of adsorbate, respectively; W (g) denotes the adsorbent mass; and V (L) refers to the solution volume. For the kinetics and thermodynamic studies, the experiments were carried out at three different adsorbent dosages (0.75, 1.25, and 1.75 g) and at four different temperatures (25°C, 30°C, 35°C, and 40°C), respectively. Table 1 shows that all kinetics, isotherm models, and thermodynamic studies were fitted to the experimental data using their linear equations.

RESULTS AND DISCUSSION

Adsorbent Characterisation

To characterise the prepared IONPs, several tests were conducted to gain insights into the prepared absorbent. Figure 1(a) shows the FESEM image that clearly demonstrates the sphericality of the IONPs particles. Each particle is composed of several smaller nanoparticles. The EDS analysis of the adsorbent verified that iron (Fe) and oxygen (O) were the primary elemental components, as illustrated in Figure 1(b), suggesting a high level of purity of the IONPs produced. The results presented here are consistent with previously reported data by Khosravi and Azizian [24]. Figure 1(c) showed the TEM images of the prepared IONPs. The images obtained were noticed similar as reported by Phu, et al. [25] during a characterisation study of amorphous iron-chromium oxide nanoparticles prepared by sonochemistry. Well-shaped spherical or ellipsoidal

Table 1. Equations of kinetics, isotherm models and thermodynamic study.

Parameters	Equation		Nomenclature
Pseudo-first order (PFO)	$\ln(q_e - q_t) = \ln q_e - K_1 t$	(3)	q_e = amount adsorbate quilibrium (mg/g) q_t = amount adsorbate retained at time (mg/g) q_m = monolayer capacity of the adsorbent (mg/g) t = time (min) k_1 = PFO rate constant (1/min) k_2 = PSO rate constant (g/mg.min) k_{ID} = IPD rate constant (mg/g/min$^{0.5}$) C_i = thickness of the boundary layer (mg/g) b = Langmuir adsorption equilibrium constant (L/mg) C_e = equilibrium concentration (mg/L) C_0 = initial concentration (mg/L) R_L = separation factor n = adsorption intensity K_F = constant relating the adsoprtion capacity (L/g) K_T = Temkin equilibrium binding constant (L/g) b_T = Temkin isotherm constant (mg/L) R = gas constant (8.314 J/mol.K) T = absolute temperature (K) q_s = theorytical saturation capacity (mg/g) k_{ad} = adsorption equilibrium constant ε = Polanyi potential B = constant related to adsorption energy (mol^{2}k/J^2) E = free energy (kJ/mol) k_D = adsorption equilibrium constant (l/mg) ΔG° = free energy (kJ/mol) ΔS° = change in enthalpy (kJ/mol) ΔH° = change in entropy (J/mol.K)
Pseudo-second order (PSO)	$t/q_t = (1/k_2 q_e^2) + (1/q_e)\,t$	(4)	
Intraparticle diffusion (IPD)	$q_t = k_{ID} t^{0.5} + C_i$	(5)	
Langmuir	$C_e/q_e = 1/bq_m + C_e/q_m$; $R_L = 1/(1 + b\,C_0)$	(6)	
Freundlich	$\ln q_e = \ln K_F + (1/n)\ln C_e$	(7)	
Temkin	$q_e = B \ln K_T + B \ln C_e$; $B = RT/b_T$	(8)	
D-R	$\ln q_e = \ln q_s - k_{ad}\,\varepsilon^2$; $\varepsilon = RT \ln\left[1 + 1/C_e\right]$; $E = 1/\sqrt{2B}$	(9)	
Thermodynamic	$\ln K_D = -\Delta G°/RT$; $\ln K_D = (\Delta S°/R) - (\Delta H°/RT)$; $\Delta G° = \Delta H° - T\Delta S°$	(10)	

iron oxide nanoparticles (IONPs) were observed in the TEM images. Figure 1(d) illustrates the particle size distributions via a histogram, which was obtained by measuring 100 nanoparticles, as recommended by Baseri and Tizro [26] and Mossa Hosseini, et al. [23]. Investigation on the diameter of 100 nanoparticles from TEM images demonstrates that the IONPs relatively had the diameter size of 40 ± 5 nm.

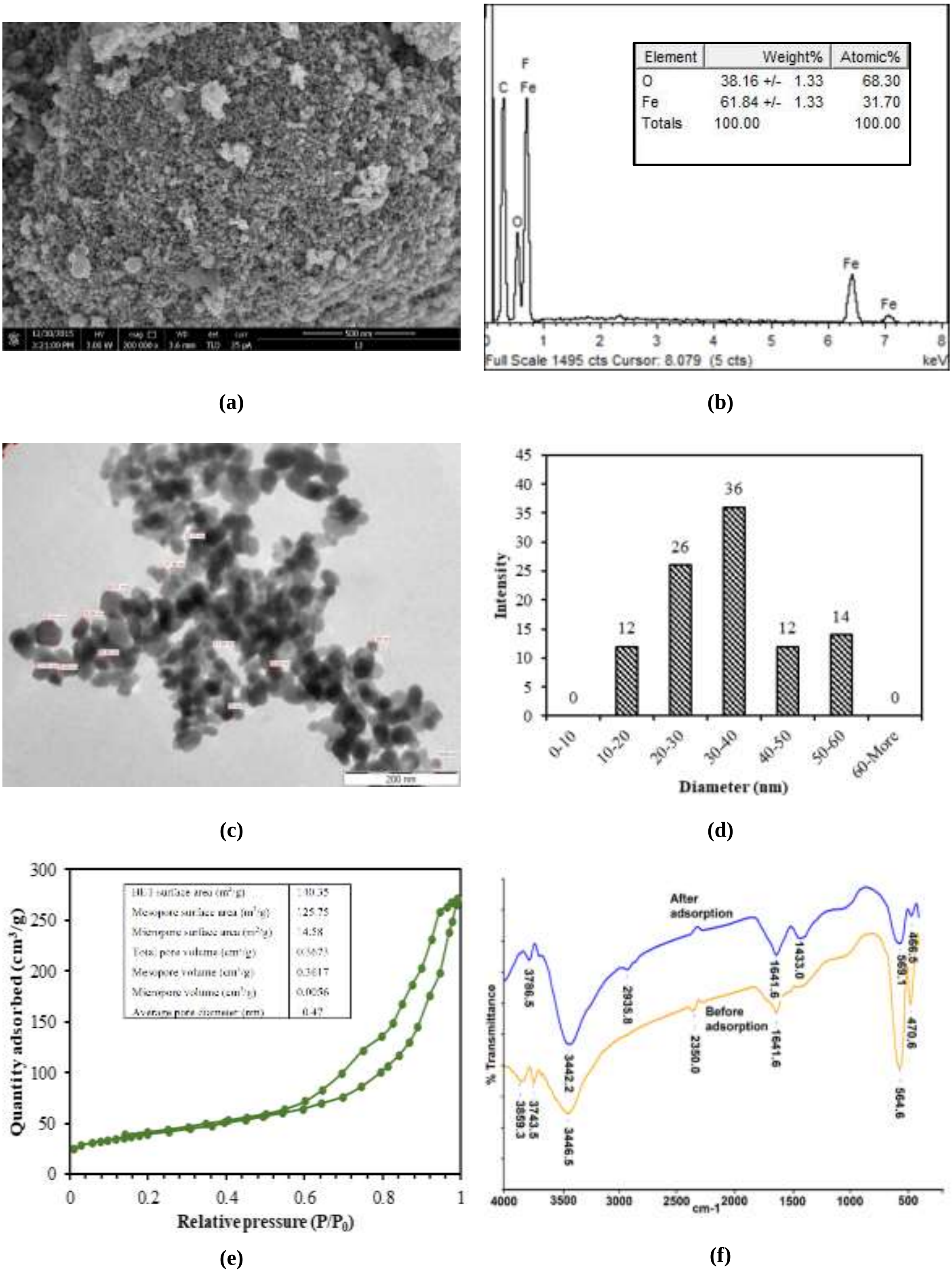

Element	Weight%	Atomic%
O	38.16 +/- 1.33	68.30
Fe	61.84 +/- 1.33	31.70
Totals	100.00	100.00

BET surface area (m²/g)	130.35
Mesopore surface area (m²/g)	125.75
Micropore surface area (m²/g)	4.58
Total pore volume (cm³/g)	0.3673
Mesopore volume (cm³/g)	0.3617
Micropore volume (cm³/g)	0.0056
Average pore diameter (nm)	0.47

(a)

(b)

(c)

(d)

(e)

(f)

Figure 1. (a) FESEM image; (b) EDS analysis result; (c) TEM image; (d) histogram of particle size distributions; (e) N_2 adsorption-desorption analysis; and (f) FTIR analysis spectrum of IONPs.

The BET surface area, total pore volume, and average pore diameter of the prepared adsorbent were 140.35 m^2/g, 0.3673 cm^3/g, and 10.47 nm, respectively. IONPs demonstrated a minimal nitrogen uptake at low relative pressure and present type II according to the IUPAC classification. The IONPs hysteresis loop was identified as H3, as the loop does not have a plateau at high (P/P_o) values. Figure 1(c) shows that the FTIR spectrum obtained for the prepared IONPs displayed the following bands: 3736 and 3617 cm^{-1} are attributed to O–H vibrations in hydroxyl groups [27], while the peak at 3431 cm^{-1} is caused by the O–H stretching vibrations of the hydroxyl group in the adsorbed water molecules [28]. Meanwhile, the absorption peak at 1635 cm^{-1} can be assigned to the C=O stretching [24]. The spectra also contained a strong band at 570 cm^{-1}, which is attributed to the stretching vibration of Fe^{3+}–O^{2-} bond in the tetrahedral position in the spinel structure. Moreover, a less intense peak at 1430 cm^{-1} can be detected, thus corresponding to the Fe^{3+}–O^{2-} bond in the octahedral position. The variation in the absorption band between the Fe^{3+}–O^{2-} bond in the octahedral and tetrahedral positions is attributed to the discrepancy in the bond length of Fe^{3+}–O^{2-} in these two positions. Several researchers, including Hung, et al. [28] and Li, et al. [29], also asserted similar findings. After adsorption, slight changes were observed, including the appearance of new peaks at the region 2936 cm^{-1} and the widening of peaks at regions 3854 and 3443 cm^{-1}, which relate to the single bond –OH and single bond Si–OH groups. Moreover, the aromatic ring is assigned to the band at 1500 to 1600 cm^{-1}. These findings are consistent with the studies reported earlier by Wang and Wang [30]. It was observed that there is a notable difference between the FTIR spectra of IONPs before and after the adsorption studies. These differences in the FTIR spectra indicate that the organic molecules have successfully attached themselves to the surface of the IONPs. This has resulted in a change in both peak position and intensity.

Kinetics Study

This present study used the pseudo-first-order (PFO) and pseudo-second-order (PSO) methods to analyse the experimental data, such as the controlling mechanisms of the adsorption process, including chemical reaction, diffusion control, and mass transfer [31]. The parameter data of PFO and PSO can be determined from the slope and intercept of the plot $\ln(q_e-q_t)$ against t and plot t/q_t against t by the linear Eq. (3) and (4), respectively. Table 3 lists the parameters obtained in the PFO and PSO equations, together with their R^2 and $q_{e,cal}$. The plot $\ln(q_e-q_t)$ against t (figure is not shown) gave a less linear relationship, resulting in a low R^2 value. Additionally, there was a significant difference between the experimental and calculated values of q_e, indicating that the experimental data did not fit well with the PFO kinetics model. However, the plot t/q_t against t (Figure 2(a)) showed a linear relationship, and the R^2 value (~0.9990) for the PSO kinetic model was relatively higher than that of the PFO. Moreover, the $q_{e,cal}$ value derived from the PSO model was close to the $q_{e,exp}$ value. Thus, these results suggest that the PSO model provided a good correlation for the adsorption of COD onto IONPs. Most of the previous studies also report PSO kinetic for adsorption, such as the adsorption of methyl orange onto pumpkin seed powder [32] and the adsorption of reactive orange by iron oxide nanospheres [24]. The PSO kinetic model also verified that the chemisorption was the rate-controlling step over the whole adsorption process [33].

The study examined the intraparticle diffusion (IPD) model as the PFO and PSO kinetic models failed to identify any diffusion mechanism [34]. IPD focuses on the diffusion of adsorbate molecules within the interior of the adsorbent particles. IPD assumes that the rate-limiting step in the adsorption process is the diffusion of the adsorbate from the external surface of the adsorbent particles into the internal pore structure. The IPD parameters (k_{ID} and C) were calculated from the plot q_t vs. $t^{1/2}$ slope and intercept, and the data are presented in Table 2. The plot q_t vs. $t^{1/2}$ (Figure 2(b)) showed multilinearity, indicating that more than one step occurs during the adsorption of dCOD. Similar adsorption patterns have been observed in previous studies. According to the study, the first portion of the plot is the instantaneous adsorption or external surface adsorption stage (Stage I). Here, the adsorbate (dCOD-contributed molecules) migrated from the solution to the exterior surface of the adsorbent (IONPs) particles due to bulk diffusion. The second portion is the gradual adsorption stage (Stage II), where the COD molecules moved within the particles due to intraparticle diffusion. In the final equilibrium stage (Stage III), the COD molecules were adsorbed at the sites on the interior surface of the IONPs. Moreover, the multilinearity observed in the plot suggests that intraparticle diffusion is not the rate-limiting step. The study observed that the value of k_{ID1} and k_{ID2} decreased with increasing adsorbent dosage from 7.5 to 17.5 g/L. Additionally, the values of k_{ID1} were found to be larger than k_{ID2} at a constant adsorbent dosage. This indicates that the adsorption was rapid at the initial stage; however, the adsorption became slower beyond this stage, and there was no further adsorption when equilibrium was achieved. The magnitude in the C_1 pattern with the changes in adsorbent dosage was not very clearly observed. However, in the second stage, it was noticed that C_2 had decreased with increased adsorbent dosage due to the higher adsorbent dosage that weakened the boundary layer effect.

Table 2. Kinetics and intraparticle parameters for the adsorption of dCOD onto IONPs.

Dosage/ volume (g/L)	$q_{e,exp}$ (mg/g)	Kinetic model					
		Pseudo first order			Pseudo second order		
		$q_{e,cal}$ (mg/g)	K_1 (1/min)	R^2	$q_{e,cal}$ (mg/g)	K_2 (g/mg min)	R^2
7.5	57.32	48.45	0.0444	0.9851	58.48	0.0028	0.9993
12.5	53.15	44.07	0.0642	0.9909	54.35	0.0043	0.9990
17.5	47.32	35.21	0.9801	0.9801	48.78	0.0043	0.9989

Dosage/ volume (g/L)	Intra-particle diffusion model					
	k_{ID1} (mg/g min$^{0.5}$)	C_1 (mg/g)	R^2	k_{ID2} (mg/g min$^{0.5}$)	C_2 (mg/g)	R^2
7.5	14.071	1.7675	0.9803	4.222	36.816	0.9573
12.5	13.392	0.5701	0.9761	4.203	30.338	0.9206
17.5	11.854	-0.6029	0.9967	3.167	27.937	0.9690

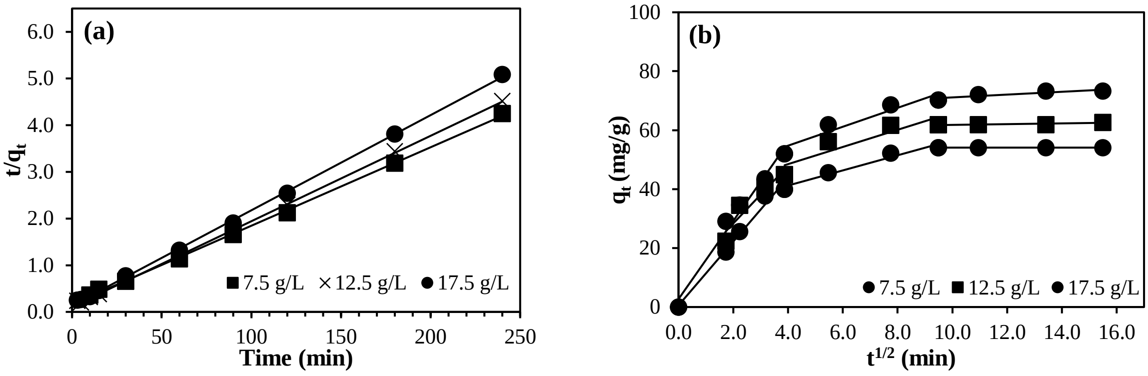

Figure 2. (a) Pseudo-second-order kinetic; and (b) Intraparticle diffusion for the adsorption of dCOD onto the IONPs.

Isotherm Study

The data obtained from the equilibrium adsorption study were analysed using four isotherm models, namely, Langmuir, Freundlich, Temkin, and D-R. These models were used to examine the adsorption behaviour in detail. The linear plot of adsorption isotherm model and the adsorption parameters based on each isotherm equation, along with a determination coefficient (R^2), are shown in Figure 3 and listed in Table 3. According to the linear regression (R^2) analysis method, it was observed that the values of the correlation coefficients were slightly high (≥0.9300). This finding shows that the results fitted these four models very well. Upon a more detailed examination of the isotherm data using root-mean-square error (RMSE) and chi-square (χ^2) analysis, it was determined that the D-R isotherm model is the most suitable for describing the adsorption of dCOD on the IONPs. This conclusion is based on the model's ability to achieve low values for both analyses. Moreover, adsorption was observed to have complied with the D-R isotherm model better than the Langmuir did due to several factors: (a) Surface heterogeneity: The D-R model is often used when the adsorbent surface is heterogeneous; (b) The D-R model can account for multilayer adsorption and is often used for adsorption on porous materials with complex pore structures; and (c) The comparison of the experimental adsorption data with the predictions of both the Langmuir and D-R models.

For the Langmuir isotherm, isotherm parameters b and q_m can be determined from the slope of the plot of C_e/q_e vs. C_e from the linear Eq. (6). In the conditions studied, the Langmuir model predicted a maximum adsorption capacity (q_m) of 69.44 mg/g. The calculated R_L value was 0.1460, which is greater than zero and less than unity, indicating favourable adsorption of dCOD onto IONPs. A previous study by Ezechi, et al. [35], claimed that for favourable adsorption, $0 < R_L < 1$; unfavourable adsorption, $R_L > 1$; linear adsorption, $R_L = 1$; and the adsorption process is irreversible if $R_L = 0$. For the Freundlich isotherm model, the values of n and K_F can be calculated from the plot of ln q_e vs. ln C_e using Eq. (7). Based on Table 3, n and K_F were found to be 4.1754 and 10.6632, respectively, with $R^2 = 0.9341$. According to Abbas and Trari [36], the Temkin isotherm represents the quantity of heat needed for the adsorption by one layer of adsorbate on the surface of the adsorbent. Temkin isotherm constants were determined from the slope and intercept of the plot of q_e vs. ln C_e from the linear Eq. (8). From Table 3, the calculated value of B was 12.61 J/mol, while that of b_T and K_t were 196.46 mg/L and 6.32×10^{-2} L/g, respectively. The adsorption energy (E) can be calculated from the plot of ε^2 vs. ln q_e using the D-R linear equation from Eq. (9). The value of q_s, K_{ad}, and E was found to be 60.38 mg/g, 1.26×10^{-3} mol^2/kJ^2, and 6.30 KJ/mol, respectively. In the case of $E < 8$ kJ/mol, physical forces may affect the adsorption [36].

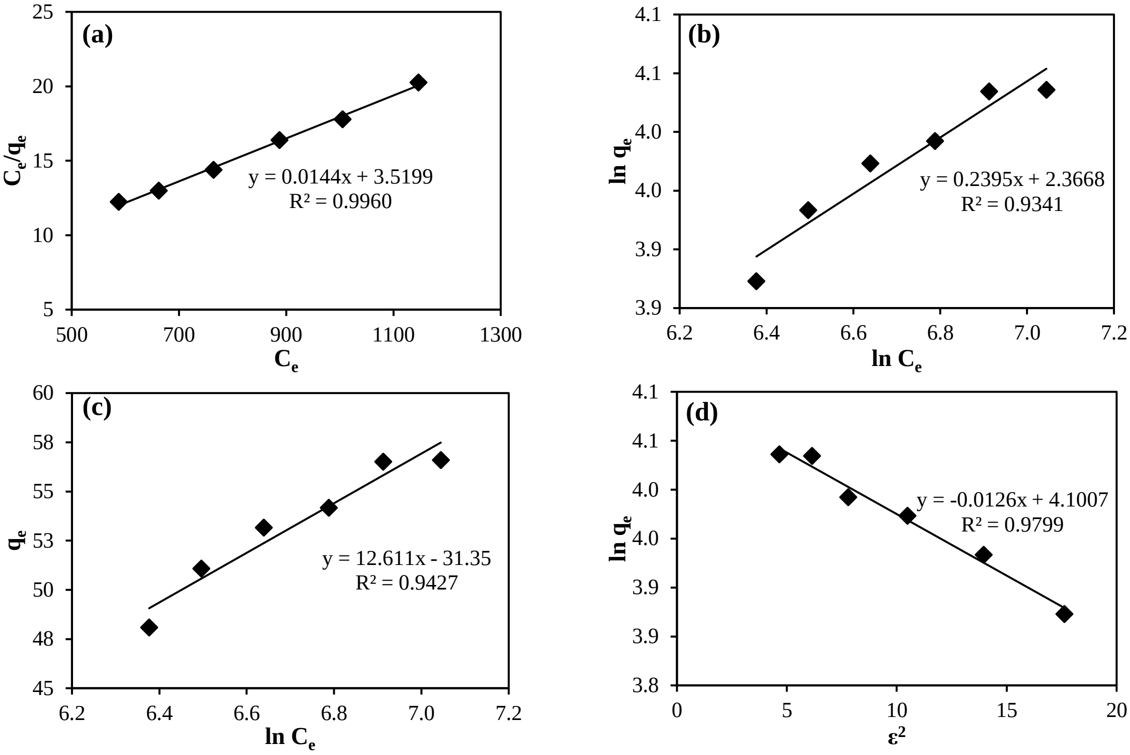

Figure 3. Plots of: (a) Langmuir; (b) Freundlich; (c) Temkin; and D-R isotherm for dCOD adsorption onto the IONPs.

Table 3. Langmuir, Freundlich, Temkin, and D-R constants for dCOD adsorption onto the IONPs.

Langmuir		Freundlich		Temkin		Dubinin-Radushkevic	
q_m (mg/g)	69.44	n	4.1754	B (J/mol)	12.61	q_s (mg/g)	60.38
b (L/mg)	4.09×10^{-3}	K_F (L/g)	10.6632	b_T (mg/L)	196.46	K_{ad} (mol^2/kJ^2)	1.26×10^{-2}
R_L	0.1460			K_t (L/g)	6.32×10^{-2}	E (KJ/mol)	6.30
R^2	0.9960	R^2	0.9341	R^2	0.9427	R^2	0.9799
RMSE	0.6151	RMSE	0.7754	RMSE	0.7191	RMSE	0.4207
χ^2	0.0434	χ^2	0.0681	χ^2	0.0587	χ^2	0.0196

Table 4. Thermodynamic study for adsorption of dCOD onto IONPS.

Temperature °C	k_{ad} (mL/g)	ΔG° (kJ/mol)	ΔH° (kJ/mol)	ΔS° (J/mol.K)
25	74.54	−10.68	1.23	39.96
30	75.13	−10.87		
35	75.36	−11.07		
40	76.47	−11.27		

Thermodynamic Study

The van 't Hoff plot (figure not shown) uses the slope and intercept of the plots of ln K_D versus 1/T to determine the values of ΔH° and ΔS°. Based on Table 4, the Gibbs free energy (ΔG°) for dCOD was found to be between −10.68 and −11.27 kJ/mol when the temperature increased from 25°C to 40°C. Meanwhile, the negative ΔG° values indicate the occurrence of a spontaneous physisorption. Moreover, the negative values of ΔG° increased with increasing temperature, suggesting more spontaneous adsorption at higher temperatures [34]. The calculated ΔH° value was 1.23 kJ/mol, which indicates that the adsorption process was endothermic. This result suggests that the adsorption was physical in nature, involving weak forces of attraction between the adsorbate and the IONPs. The low value of ΔH° (less than 40 kJ/mol) implies that there was loose bonding between the adsorbate molecules and the adsorbent surface. In the case of entropy (ΔS°), it was found to be 39.96 J/mol.K. The positive value of ΔS° resulted from the increased randomness due to the adsorption of dCOD, which suggested good affinity of the solute molecule towards the IONPs and increased randomness at the solid-solution interface during the fixation of organic solute on the active site of the adsorbent [34]. A similar finding was also reported by Adane, et al. [37].

CONCLUSION

The current investigation indicates that IONPs is a promising adsorbent for reducing dCOD from landfill leachate. The equilibrium data were fitted to various isotherms, such as Langmuir, Freundlich, Temkin, and D-R. However, the D-R isotherm model was found to be the best fit. Using Langmuir model, the maximum monolayer adsorption was calculated to be 21.74 mg/g. Thermodynamic parameters, such as free energy changes (ΔG°), enthalpy (ΔH°), and entropy (ΔS°), were evaluated between 25°C and 40°C. The ΔG° decreased progressively from −10.68 kJ/mol to −11.27 kJ/mol as the temperature increased. The ΔH° and ΔS° values were found to be 1.23 kJ/mol and 39.96 J/mol.K, respectively. The results indicate that the overall adsorption process was endothermic and spontaneous. The findings suggest that IONPs could be a viable adsorbent in managing higher dCOD problems associated with landfill leachate.

ACKNOWLEDGEMENTS

This research was financially supported by the Universiti Teknologi MARA through MyRA Research Grant-Lepasan PhD (LPhD), 600-RMC/GPM LPHD 5/3 (183/2021). Great appreciation goes to Universiti Sains Malaysia and Ministry of Higher Education (MOHE) for providing the support throughout the completion of this research.

REFERENCES

1. Solanki, A., Kumar, D. and Sharma, P. (2024) A mini-review on agro waste mediated technologies used for landfill leachate treatment. *Journal of Water Process Engineering*, **57**, 104685.

2. Abuabdou, S. M. A., Ahmad, W., Aun, N. C. and Bashir, M. J. K. (2020) A review of anaerobic membrane bioreactors (AnMBR) for the treatment of highly contaminated landfill leachate and biogas production: Effectiveness, limitations and future perspectives. *Journal of Cleaner Production*, **255**, 120215.

3. Ghani, Z. A, Yusoff, M. S., Alazaiza, M. Y. D., Akinbile, C. O. and Abd Manan, T. S. (2023) Landfill leachate treatment by activated carbon (AC) from banana pseudo-stem, iron oxide nanocomposite (IOAC), and iron oxide nanoparticles (IONPs). *Journal of Environmental Chemical Engineering*, **11(3)**, 110132.

4. Zamri, M. F. M. A, Kamaruddin, M., Yusoff, M., Aziz, H. and Foo, K. (2015) Semi-aerobic stabilized landfill leachate treatment by ion exchange resin: isotherm and kinetic study. *Applied Water Science*, 1–10.

5. Shehzad, A., Bashir, M. J. K., Sethupathi, S., and Lim, J. W. (2015) An overview of heavily polluted landfill leachate treatment using food waste as an alternative and renewable source of activated carbon. *Process Safety and Environmental Protection*, **98**, 309–318.

6. Ghani, Z. A., Yusoff, M. S., Zaman, N. Q., Zamri, M. F. M. A. and Andas, J. (2017) Optimization of preparation conditions for activated carbon from banana pseudo-stem using response surface methodology on removal of color and COD from landfill leachate. *Waste Management*, **62**, 177–187.

7. Ibrahim, A. and Yaser, A. Z. (2019) Colour removal from biologically treated landfill leachate with tannin-based coagulant. *Journal of Environmental Chemical Engineering*, **7(6)**, 103483.

8. Poblete, R. and Pérez, N. (2020) Use of sawdust as pretreatment of photo-Fenton process in the depuration of landfill leachate. *Journal of Environmental Management*, **253**, 109697.

9. de Souza Marotta Alfaia, R. G., de Almeida, R., Soares do Nascimento, K. and Carbonelli Campos, J. (2023) Landfill leachate pretreatment effects on nanofiltration and reverse osmosis membrane

performance. *Process Safety and Environmental Protection*, **172**, 273–281.

10. Chen, W. and Li, Q. (2020) Elimination of UV-quenching substances from MBR- and SAARB-treated mature landfill leachates in an ozonation process: A comparative study. *Chemosphere*, **242**, 125256.

11. Yang, X., Chen, C., Zhang, T., Tian, X., Zhang, R., Manhaeghe, D., Zhao, Y., Song, S., Demeestere, K. and Van Hulle, S. W. H. (2023) Low-cost mineral packing materials improve DOM and micropollutants removal from landfill leachate in ozonation bubble columns: Insights into the enhancement mechanisms and applicability of surrogate-based monitoring. *Chemical Engineering Journal*, **458**, 141461.

12. Labiadh, L., Fernandes, A., Ciríaco, L., Pacheco, M. J., Gadri, A., Ammar, S. and Lopes, A. (2016) Electrochemical treatment of concentrate from reverse osmosis of sanitary landfill leachate. *Journal of Environmental Management*, **181**, 515–521.

13. Jegadeesan, C., Somanathan, A. and Jeyakumar, R. B. (2023) Sanitary landfill leachate treatment by aerated electrochemical Fenton process. *Journal of Environmental Management*, **337**, 117698.

14. Viegas, C., Nobre, C., Mota, A., Vilarinho, C., Gouveia, L. and Gonçalves, M. (2021) A circular approach for landfill leachate treatment: Chemical precipitation with biomass ash followed by bioremediation through microalgae. *Journal of Environmental Chemical Engineering*, **9(3)**, 105187.

15. Aftab, B., Cho, J., Shin, H. S. and Hur, J. (2020) Using EEM-PARAFAC to probe NF membrane fouling potential of stabilized landfill leachate pretreated by various options. *Waste Management*, **102**, 260–269.

16. Scandelai, A. P. J., Zotesso, J. P., Jegatheesan, V., Cardozo-Filho, L. and Tavares, C. R. G. (2020) Intensification of supercritical water oxidation (ScWO) process for landfill leachate treatment through ion exchange with zeolite. *Waste Management*, **101**, 259–267.

17. Arias-Paic, M., Cawley, K. M., Byg, S. and Rosario-Ortiz, F. L. (2016) Enhanced DOC removal using anion and cation ion exchange resins. *Water Research*, **88**, 981–989.

18. Santhosh, C., Velmurugan, V., Jacob, G., Jeong, S. K., Grace, A. N. and Bhatnagar, A. (2016) Role of nanomaterials in water treatment applications: A review. *Chemical Engineering Journal*, **306,** 1116–1137.

19. Pillai, P., Dharaskar, S., Sinha, M. K., Sillanpää, M. and Khalid, M. (2020) Iron oxide nanoparticles modified with ionic liquid as an efficient adsorbent for fluoride removal from groundwater. *Environmental Technology & Innovation*, **19**, 100842.

20. Jawed, A., Golder, A. K. and Pandey, L. M. (2023) Synthesis of iron oxide nanoparticles mediated by Camellia sinensis var. Assamica for Cr(VI) adsorption and detoxification. *Bioresource Technology*, **376**, 128816.

21. Akhtar, M., Hussain, M., Naeem, F., Akhter, P., Jamil, F., Qamar, O. A., Bazmi, A. A., Tariq, N., Asrar, A. and Park, Y. K. (2023) Green and sustainable synthesis of iron oxide nanoparticles for synergetic removal of melanoidin from ethanol distillery simulated model wastewater. *Journal of Industrial and Engineering Chemistry*.

22. APHA (2012) Standard Methods for the Examination of Water and Wastewater 22 ed. 2012, Washington, DC, New York: APHA, AWWA, WPCF.

23. Mossa Hosseini, S., Ataie-Ashtiani, B. and Kholghi, M. (2011) Nitrate reduction by nano-Fe/Cu particles in packed column. *Desalination*, **276(1–3)**, 214-221.

24. Khosravi, M. and Azizian, S. (2014) Adsorption of anionic dyes from aqueous solution by iron oxide nanospheres. *Journal of Industrial and Engineering Chemistry*, **20(4)**, 2561–2567.

25. Phu, N. D., Sy, T. X., Cao, H. T., Dinh, N. N., Thien, L. V., Hieu, N. M., Nam, N. H. and Hai, N. H. (2012) Amorphous iron-chromium oxide nanoparticles prepared by sonochemistry. *Journal of Non-Crystalline Solids*, **358(3)**, 537–543.

26. Baseri, H. and Tizro, S. (2017) Treatment of nickel ions from contaminated water by magnetite based nanocomposite adsorbents: Effects of thermodynamic and kinetic parameters and modeling with Langmuir and Freundlich isotherms. *Process Safety and Environmental Protection*, **109**, 465–477.

27. Huang, X., Schmucker, A., Dyke, J., Hall, S. M., Retrum, J., Stein, B., Remmes, N., Baxter, D. V., Dragnea, B. and Bronstein, L. M. (2009) Magnetic nanoparticles with functional silanes: evolution of well-defined shells from anhydride containing silane. *J. Mater. Chem.*, **19(24)**, 4231–4239.

28. Hung, D. Q., Dinh, L. X., Van Tung, N., Huong, L. T. M., Lien, N. T., Minh, P. T. and Le, T. H.

(2023) The adsorption kinetic and isotherm studies of metal ions (Co^{2+}, Sr^{2+}, Cs^{+}) on Fe_3O_4 nanoparticle of radioactive importance. *Results in Chemistry*, **6**, 101095.

29. Li, Z., Qiang, L., Zhong, S., Wang, H. and Cui, X. (2013) Synthesis and characterization of monodisperse magnetic Fe_3O_4@BSA core–shell nanoparticles. *Colloids and Surfaces A: Physicochemical and Engineering Aspects*, **436**, 1145–1151.

30. Wang, C. and Wang, H. (2018) Pb(II) sorption from aqueous solution by novel biochar loaded with nano-particles. *Chemosphere*, **192**, 1–4 (Supplement C).

31. Ghani, Z. A., Yusoff, M. S., Zaman, N. Q., Andas, J. and Aziz, H. A. (2017) Adsorptive removal of dissolved organic matter (DOM) in landfill leachate by iron oxide nanoparticles (FeONPs). *AIP Conference Proceedings*, **1892(1)**, 040016.

32. Subbaiah, M. V. and Kim, D. S. (2016) Adsorption of methyl orange from aqueous solution by aminated pumpkin seed powder: Kinetics, isotherms, and thermodynamic studies. *Ecotoxicology and Environmental Safety*, **128**, 109–117.

33. Zhu, C. S., Wang, L. P. and Chen, W. B. (2009) Removal of Cu(II) from aqueous solution by agricultural by-product: Peanut hull. *Journal of Hazardous Materials*, **168(2–3)**, 739–746.

34. Tcheka, C., Conradie, M. M., Assinale, V. A. and Conradie, J. (2024) Mesoporous biochar derived from Egyptian doum palm (Hyphaene thebaica) shells as low-cost and biodegradable adsorbent for the removal of methyl orange dye: Characterization, kinetic and adsorption mechanism. *Chemical Physics Impact*, **8**, 100446.

35. Ezechi, E. H., Kutty S. R. B. M., Malakahmad, A. and Isa, M. H. (2015) Characterization and optimization of effluent dye removal using a new low cost adsorbent: Equilibrium, kinetics and thermodynamic study. *Process Safety and Environmental Protection*, **98**, 16–32.

36. Abbas, M. and Trari, M. (2015) Kinetic, equilibrium and thermodynamic study on the removal of Congo Red from aqueous solutions by adsorption onto apricot stone. *Process Safety and Environmental Protection*, **98**, 424–436.

37. Adane, B., Siraj, K. and Meka, N. (2015) Kinetic, equilibrium and thermodynamic study of 2-chlorophenol adsorption onto Ricinus communis pericarp activated carbon from aqueous solutions. *Green Chemistry Letters and Reviews*, **8(3-4)**, 1–12.